Electron trapping in ferroelectric HfO_2

Roman A. Izmailov,[1,*] Jack W. Strand,[2,3] Luca Larcher,[4]
Barry J. O'Sullivan,[5] Alexander L. Shluger,[3] and Valeri V. Afanas'ev[1]

[1]*Katholieke Universiteit Leuven, Celestijnenlaan 200d, Leuven 3001, Belgium*
[2]*Università di Modena e Reggio Emilia, Via Amendola 2, Reggio Emilia 42122, Italy*
[3]*University College London, Gower Street, London WC1E 6BT, United Kingdom*
[4]*Applied Materials, Via Meuccio Ruini 9, Reggio Emilia 42122, Italy*
[5]*imec, Kapeldreef 75, Leuven 3001, Belgium*

(Received 17 November 2020; revised 12 February 2021; accepted 3 March 2021; published 23 March 2021)

Charge trapping study at 300 and 77 K in ferroelectric (annealed Al- or Si-doped) and nonferroelectric (unannealed and/or undoped) HfO_2 films grown by atomic layer deposition reveals the presence of "deep" and "shallow" electron traps with volume concentrations in the 10^{19}-cm^{-3} range. The concentration of deep traps responsible for electron trapping at 300 K is virtually insensitive to the oxide doping by Al or Si but slightly decreases in films crystallized by high-temperature annealing in oxygen-free ambient. This behavior indicates that the trapping sites are intrinsic and probably related to disorder in HfO_2 rather than to the oxygen deficiency of the film. Electron injection at 77 K allowed us to fill shallow electron traps energetically distributed at ~0.2 eV. These electrons are mobile and populate states with thermal ionization energies in the range ~0.6–0.7 eV below the HfO_2 conduction band (CB). The trap energy depth and marginal sensitivity of their concentration to crystallization annealing or film doping with Si or Al suggests that these traps are associated with boundaries between crystalline grains and interfaces between crystalline and amorphous regions in HfO_2 films. This hypothesis is supported by density functional theory calculations of electron trapping at surfaces of monoclinic, tetragonal, and orthorhombic phases of HfO_2. The calculated trap states are consistent with the observed thermal ionization (0.7–1.0 eV below the HfO_2 CB) and photoionization energies (in the range of 2.0–3.5 eV below the HfO_2 CB) and support their intrinsic polaronic nature.

DOI: 10.1103/PhysRevMaterials.5.034415

I. INTRODUCTION

In recent years ferroelectric (FE) HfO_2-based insulating layers have attracted significant attention because the ferroelectricity, associated with the oxide crystallization in noncentrosymmetric orthorhombic phase, can be achieved in films of only several nanometers in thickness [1] enabling fabrication of deep-scaled electron devices. In particular, FE field effect transistors (FE-FETs) in which information is stored in the form of polarization of the FE gate insulator, are compatible with the mainstream Si complementary metal-oxide semiconductor technology [2,3] and, therefore, can easily be implemented, and this continues to be scaled. However, HfO_2 layers are long known to suffer from significant electron trapping [4,5] leading to threshold voltage instability which greatly impairs the FET reliability [6,7]. In FE-FETs the problem becomes even more acute because of the high coercive field in FE-HfO_2 facilitating electron injection and larger thickness of the oxide layer (typically in the range 5–10 nm) than in the scaled FETs in logic circuits. The charge trapping effectively compensates the electric field induced by the FE polarization and may eventually overrun the FE behavior if using polarizing pulses of large amplitude [8]. This mandates the search for possible technological ways to reduce the electron trap density prompting quantification of electron trap density in HfO_2 layers and establishing their atomic nature.

In the present work we compared electron trapping properties of FE HfO_2 layers stabilized by Al(5.5%) or Si(3.6%) doping to the non-FE undoped HfO_2 films grown by atomic layer deposition (ALD). Experiments conducted at room temperature and at 77 K enabled determination of electron trap density both deep in the oxide gap and near the HfO_2 conduction band (CB) bottom edge. The trap densities appear to be comparable in FE and non-FE HfO_2, i.e., insensitive to the presence of dopants, suggesting their intrinsic nature. One may consider oxygen vacancies as dominant defects in HfO_2 since their concentration is expected to be enhanced upon high temperature post deposition annealing (PDA) in O-free ambient. Furthermore, O scavenging from the underlying HfO_2 layer by the TiN-based top electrodes is possible at even lower temperatures than used in the present work [9] leading to higher O deficiency in HfO_2 layers. However, the observed reduction of trap density with annealing temperature in O-free ambient allows one to exclude the O deficiency of HfO_2 as the main source of electron trapping. It is worth mentioning that electron spin resonance (ESR) measurements have been done on such samples but revealed no paramagnetic signal from HfO_2, either prior or after electron injection from the Si substrate. The only observed ESR signal that was tentatively associated with the O-vacancy in HfO_2 (based on comparison to the *ab initio* calculations of *g* values) correlates

*roman.izmailov@kuleuven.be

 ©2021 American Physical Society

with irradiation-induced positive charging of the oxide [10]. Rather, the observed annealing-dependent behavior supports the earlier proposed relationship of deep traps (optical depth 2–4 eV) to polaronic states [11,12] formed in disordered regions of HfO_2, such as remaining inclusions of amorphous phase. Moreover, the DFT modeling presented here suggests that numerous traps with thermal ionization energies of ∼0.6–1.0 eV may be associated with boundaries between crystalline grains and interfaces between crystalline and amorphous regions in HfO_2 films.

II. METHODOLOGY

A. Experiment

Samples were fabricated by ALD of 9.5-nm-thick HfO_2 layers from $HfCl_4$ and H_2O precursors at 300 °C on top of 7.5-nm-thick SiO_2 layers thermally grown on low doped *p*-type (100)Si substrates ($N_a \sim 10^{15}\,\mathrm{cm}^{-3}$). The SiO_2 layer serves as a tunnel oxide to allow electron injection from Si into HfO_2 to fill the traps. The ferroelectric phase of HfO_2 was stabilized by including several cycles of Al or Si precursor resulting in the doped (5.5%) Al:HfO_2 and (3.5%) Si:HfO_2 films. All samples initially received a protective top electrode stack comprised of 10 nm TiN and 50 nm polycrystalline Si deposited on top of HfO_2. In order to investigate the impact of crystallization on HfO_2 trapping properties, the samples were studied in the as-deposited state (largely amorphous Al-doped HfO_2 and undoped "reference" layers) and after crystallization annealing in N_2 at 850 °C for 60 s (Al-doped HfO_2 and the undoped HfO_2 reference) or at 1000 °C for 30 s (Si-doped HfO_2 and the undoped HfO_2 reference). To allow for optical input to the HfO_2 film, the top electrode stack was removed by wet etching and replaced by semitransparent (15 nm thick) gold electrodes of ≈0.5 mm^2 area deposited by thermoresistive evaporation of Au in high vacuum.

Electron traps in HfO_2 layers were characterized by first injecting electrons from Si followed by a 100-kHz capacitance-voltage (CV) curve recording. The 100-kHz frequency was chosen for two reasons. First, to remain in the high frequency limit of CV measurements and exclude the possible impact of Si/SiO_2 interface states on the flat-band capacitance (at least for room temperature experiments). Second, it ensures that impact of series (contact) resistance of the semitransparent top metal electrode remains negligible. Electrons were injected by applying a positive voltage pulse to the gold electrode of the MOS capacitor sufficient for electron tunneling across the SiO_2 barrier while illuminating the sample by visible light in order to produce sufficient concentration of electrons at the surface of Si. The charging pulse time (∼500 ms) was chosen to be definitely larger than the trapping kinetics saturation time to ensure the maximal filling of the traps and "decouple" the capture cross-section effects from the available trap concentration. Potentially, one can estimate the capture cross section of electron traps from the trapped charge versus injection charge dependence provided the injection current lateral uniformity is guaranteed (see, e.g., Ref. [4]). The latter is not guaranteed in the case of tunnel injection in ferroelectric HfO_2 because of polycrystalline film structure which precluded the trapping kinetics analysis in the present work. At the same time, the small thickness of the FE-HfO_2 films precludes use of laterally uniform optical generation implemented in the above indicated publication.

The injection-induced shift of the CV curve was used to quantify the trapped electron density as described elsewhere [11,12]. Next, the evolution of the trapped electron density with time has been monitored in darkness or under monochromatic illumination to evaluate the energy distribution of trapped electrons using exhaustive photodepopulation spectroscopy (EPDS) [13–15]. It has been repeatedly noticed that after electron injection pulse the density of trapped electrons significantly decreases even without optical excitation in samples stored in darkness at 300 K, indicating a high density of relatively shallow electron traps in HfO_2 with thermal ionization energies <0.5 eV. Therefore, we extended the injection experiments to low temperatures ($T \geqslant 77$ K) to evaluate the density and energy distribution of these electron traps.

As in the case of room temperature experiments, charging at 77 K was performed by applying a long (≈500 ms) positive voltage pulse to the semitransparent top electrode of MOS capacitor. An additional illumination of the sample was needed to generate sufficient density of minority carriers (electrons) near the *p*-Si/SiO_2 interface to allow their tunnel injection into the oxide stack. Long pulse time (≈500 ms) ensured that the charging process reaches saturation, i.e., all available traps are filled. Using the incremental charging pulse amplitudes V_{charging}, the CV curve shift was measured (the flat-band voltage V_{fb} or the voltage corresponding to 50% of accumulation capacitance) to monitor the density of trapped electrons.

Analysis of deep traps at room temperature was performed as described previously [11,16] after filling the maximal trap density by electron tunneling from Si. After applying the filling pulse, the samples were left in the dark for at least 48 hours to empty all shallow traps available for thermal detrapping. The CV curve shift after this "ageing" reflects the total amount of electrons stably trapped in HfO_2. Based on the spectral charge density (or SCD, defined as the density of charge lost after optical excitation by photons with the specified energies between $h\nu$ and $h\nu + \Delta h\nu$) energy distribution, these electrons have been previously shown to have photoionization energies into mobility edge states in the HfO_2 conduction band (CB) in the range of 2.0–3.5 eV (cf. Fig. 1 in [16]). SCD distribution can be directly inferred from the illumination induced change in the trapped charge density ΔQ (or the corresponding flat-band voltage shift, ΔV_{fb}), as can be seen from the following equation [11–16]:

$$\mathrm{SCD} = \frac{\Delta Q}{\Delta h\nu\, d_{\mathrm{HfO_2}}\, A\, q} = -\frac{1}{\Delta h\nu\, d_{\mathrm{HfO_2}}\, A\, q}\frac{[\mathrm{EOT(HfO_2)} + d_{\mathrm{SiO_2}}]}{\mathrm{EOT(HfO_2)}}\Delta V_{\mathrm{fb}} C_{\mathrm{ox}}, \quad (1)$$

where A stands for the capacitor area (∼0.5 mm^2), q is the elementary charge, the oxide capacitance (C_{ox}) value is determined from 100-kHz CV measurements, and effective oxide thickness (EOT) of HfO_2 layers is defined as $\mathrm{EOT(HfO_2)} = d_{\mathrm{HfO_2}} k_{\mathrm{HfO_2}} / k_{\mathrm{SiO_2}}$. In the following SCD calculations the same permittivity value ($k = 20$) was used for HfO_2 films as ca-

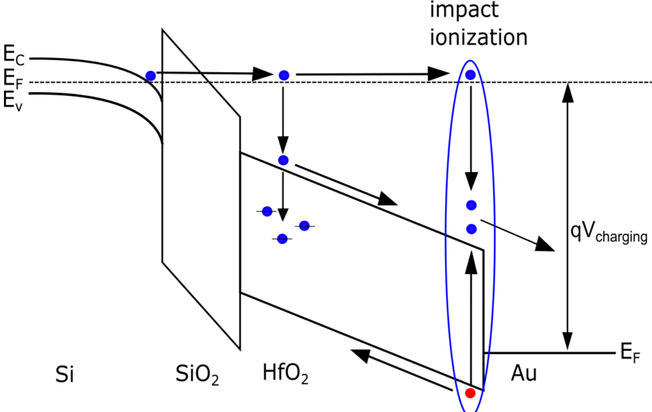

FIG. 1. Schematics of electron transitions during electron tunneling injection from Si into SiO_2/HfO_2 dielectric stack when applying positive charging pulse $V_{charging}$ to the top gold electrode of the MOS capacitor.

pacitance variation between different samples was considered to remain insignificant (within 10–20% accuracy limit). By plotting the inferred SCD values versus photon energy after each illumination step one obtains a bar plot reflecting the energy distribution of the trapped electron density.

The low temperature (77 K) HfO_2 charging and the trapped electron density monitoring have been done similarly to those at 300 K. The major difference concerns electron detrapping experiments in which, instead of *optical* excitation used in EPDS, *thermal* excitation was used by heating up the sample to room temperature. From the observed temperature-dependent CV curve shift one can estimate the trapped charge loss due to thermal excitation of captured electrons from the trap levels to the HfO_2 CB. It should be noted, however, that one also should take into account the possible effect of impact ionization. In particular, as illustrated in Fig. 1, during electron tunnel injection from silicon substrate, the applied voltage (usually in the range from +13 to +18 V) significantly exceeds the band gap of HfO_2 (about 5.6–5.9 eV [17]). This may cause generation of holes in the valence band (VB) of hafnia by impact ionization. These holes are probably initially "frozen" at 77 K and become mobile during the temperature ramp up and may efficiently annihilate electrons trapped in the oxide. To enable separation between these two processes, i.e., thermal detrapping of electrons and annihilation with holes which become mobile in the HfO_2 VB upon heating, measurements were repeated under opposite polarities of the bias voltage V_{hold}, applied to the top metal electrode during sample heating from 77 to 300 K.

This approach is illustrated by band diagrams of MOS capacitors shown in Fig. 2 for two biasing conditions: In the case of a positive bias $V_{hold} = V_{fb} > 0$ V [Fig. 2(a)] the efficient annihilation process can be expected because "unfrozen" holes are pulled through the whole HfO_2 film. By contrast, in the case of a negative bias $V_{hold} = -5$ V [Fig. 2(b)] the holes will be collected at the gold electrode, thereby revealing the "intrinsic" electron detrapping properties.

On the basis of the above considerations, the low temperature charge injection and detrapping experiments described below were conducted using the following protocol:

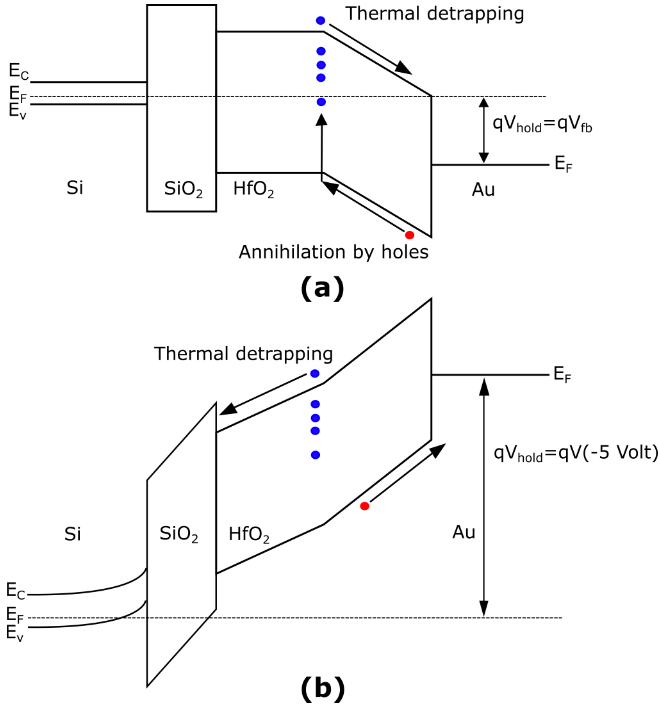

FIG. 2. Schematics of electron transition during thermal detrapping in SiO_2/HfO_2 insulating stack when applying positive (a) and negative (b) voltages V_{hold} to the top gold electrode of the MOS capacitor during temperature ramp up from 77 to 300 K.

(i) Control 100-kHz CV curves of the uncharged sample were recorded at room temperature and after cooling to 77 K.

(ii) Charging was done at 77 K (charging pulse amplitude was set to achieve maximal trapped electron density) and the after-charging CV curve was recorded.

(iii) The sample was left for 4–5 h at 77 K under zero bias to reach the stable trapped charge density level as monitored by CV curves.

(iv) The sample was biased to $V_{hold} = -5$ V or to $V_{hold} = V_{fb} > 0$ at 77 K and allowed to slowly ($\approx$1 K/min) warm up to room temperature while keeping the bias applied and monitoring the CV curve shift as a function of the sample temperature.

(v) The final CV curve was recorded at room temperature to evaluate the density of the remaining charge corresponding to electrons stably trapped on deep traps.

B. DFT calculations

Density functional theory (DFT) calculations were carried out using the CP2K package [18]. We used a hybrid DFT functional PBE0-TC-LRC [19], which mixes a percentage of nonlocal (Hartree-Fock) exchange into the exchange-correlation (XC) functional in order to improve the description of electronic structure and localized states, both of which are necessary for our purposes. This functional is derived from the standard PBE0 functional and uses 25% of Hartree-Fock (HF) exchange. For computational efficiency the HF exchange is truncated by a cutoff radius of 4 Å, beyond which the exchange interaction is calculated within a generalized gradient approximation (GGA). We used a DZVP basis set [20]

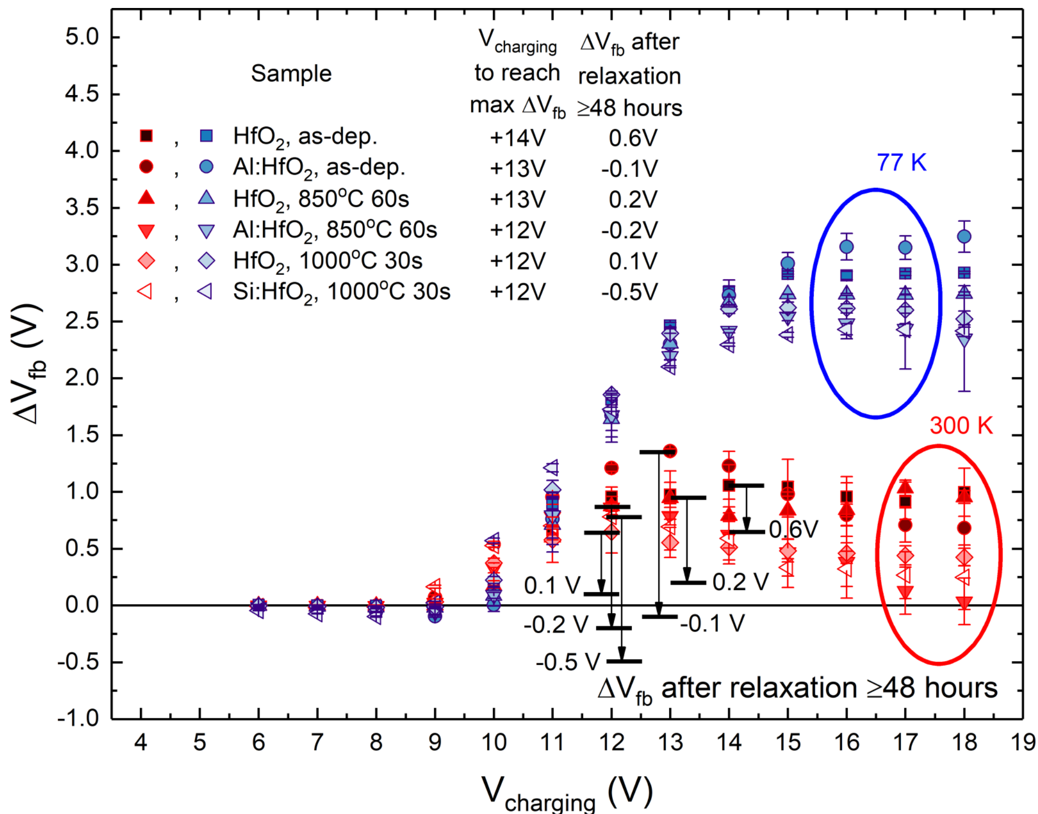

FIG. 3. V_{fb} shift vs $V_{charging}$ as measured at room temperature and at 77 K on (doped) HfO_2 samples with and without annealing. The V_{fb} shift is calculated relative the V_{fb} value measured before charging at 300 or 77 K respectively. For charging at room temperature, the V_{fb} shift remaining after ⩾48 h relaxation is indicated in the legend and shown by black arrows on the graph. Negative remaining V_{fb} shift indicates presence of trapped electrons in as-fabricated films.

and Goedecker, Teter, and Hutter pseudopotentials [21]. HF calculations are accelerated using the auxiliary density matrix method (ADMM) [22].

To study the energetics of electron traps in polycrystalline HfO_2, we considered how polaronic states form at surfaces of three phases of crystalline HfO_2. This is justified in more detail below. Surfaces are described in a slab model. Since we look at different surfaces of different crystal phases, the slab models vary in size. In all cases we have used at least a 3×3 supercell extension in the $\underline{\mathbf{a}}$ and $\underline{\mathbf{b}}$ (in-plane) directions. All slab models also contain at least 324 atoms. These slabs are translated in the $\underline{\mathbf{c}}$ direction with 30 Å vacuum between the slabs.

The thermal stability of traps is evaluated by comparing the total energies of a periodic cell with an extra electron in its delocalized state and in a localized polaronic state. The electron trapping energy E_{tr}, is defined as

$$E_{tr} = E_{deloc} - E_{loc}. \tag{2}$$

Here E_{deloc} is the cell total energy calculated with the electron in the perfect surface state, extended over the surface slab. E_{loc} is the total energy of the system with the electron in its localized state, with the atomic geometry fully relaxed. Trapping energy is large for more stable (“deeper”) trap states and corresponds to the *thermal* ionization energy of the trapped electron into the bottom of CB states.

III. RESULTS AND DISCUSSION

A. Experimental results

1. Electron injection study

The V_{fb} shift vs $V_{charging}$ curves measured at 300 K (red symbols) and 77 K (blue symbols) are compared in Fig. 3 for as-deposited and annealed samples, both Al or Si doped and the undoped HfO_2 references. At both temperatures the flat-band voltage shift was calculated as the difference between V_{fb} values measured exactly before and after electron injection, i.e., $\Delta V_{fb} = V_{fb\,final} - V_{fb\,initial}$. A several times higher V_{fb} shift during low temperature charge injection indicates that at 77 K electron trapping is dominated by shallow traps. At both temperatures the charge injection from Si is essentially limited by the breakdown of the tunnel SiO_2 layer which prevents application of the higher charging pulse because of the used charging current compliance limit (3.2 mA). This may explain the distribution in the V_{fb} shift between identically processed test structures (shown as error bars in Fig. 3) as well as between as-deposited and annealed samples, since the samples annealed at higher temperature tend to experience earlier breakdown of the tunnel SiO_2 layer at room temperature. On the other hand, at 77 K the resistance of the tunnel SiO_2 to dielectric breakdown increases and the difference between as-deposited and annealed samples becomes less pronounced (maximum V_{fb} shift is observed at the same charging pulse amplitude $V_{charging} = +15\,\text{V}$ for almost

all samples). The observed decrease in the V_{fb} shift values at higher charging pulse amplitudes may be explained by partial field-induced detrapping of the shallow trapped electrons and/or annihilation of the trapped electron charges by holes generated in HfO_2 due to impact ionization (cf. Fig. 1). Electron trapping seems to be relatively insensitive to the doping of HfO_2 films; the observed deviations may simply result from permittivity variation and/or differently occuring SiO_2 breakdown.

The density of thermally stable deep traps can be inferred from the V_{fb} shift measured after filling the traps (at room temperature) followed by at least 48 h relaxation in the dark. As shown in Fig. 3, the V_{fb} shift of ≈0.6 V, which corresponds to the concentration of traps of $\approx 1.5 \times 10^{19}\,\text{cm}^{-3}$ (assuming uniform distribution across the thickness of the high-k oxide layer; see Ref. [14] for detailed description) remains after relaxation as measured on the as-deposited undoped sample. Meanwhile a much smaller remaining V_{fb} shift is encountered for the annealed undoped samples (≈0.2 V for the samples annealed at 850 °C for 60 s and ≈0.1 V for the samples annealed at 1000 °C for 30 s). The latter correspond to the density of traps of $\approx 0.5 \times 10^{19}\,\text{cm}^{-3}$ and $\approx 0.25 \times 10^{19}\,\text{cm}^{-3}$, respectively. That proves that deep traps in undoped HfO_2 can be effectively eliminated upon annealing, probably due to the oxide crystallization which would reduce the volume fraction of amorphous or disordered hafnia in the film [12,16]. As for doped samples, even lower remaining V_{fb} shift values are observed after ⩾48 h relaxation in the dark, reaching negative V_{fb} shift values. This suggests the presence of deeply trapped electrons in as-fabricated films, which are then effectively annihilated during charging pulse due to impact ionization (cf. Fig. 1). The contribution of this fixed charge to the observed V_{fb} shift after 48 h relaxation may bring inaccuracy in determination of the density of stable deep traps based solely on charge injection experiments. Therefore, this issue is addressed specifically in the section describing the photodepopulation experiments.

The maximum values of V_{fb} shift in as-charged samples correspond to a total amount of traps that may affect device performance for short switching pulse times usually ranging from several nanoseconds to hundreds of microseconds. In undoped samples at 300 K this value varies from $\approx 2.6 \times 10^{19}\,\text{cm}^{-3}$ in unannealed samples to $\approx 2.3 \times 10^{19}\,\text{cm}^{-3}$ and $\approx 1.5 \times 10^{19}\,\text{cm}^{-3}$ in the samples annealed at 850 and 1000 °C, respectively. Similar values are observed at 300 K for the doped samples: $\approx 2.1 \times 10^{19}\,\text{cm}^{-3}$ for Al:HfO_2 samples annealed at 850 °C and $\approx 1.9 \times 10^{19}\,\text{cm}^{-3}$ Si:HfO_2 samples annealed at 1000 °C. At the same time as-deposited Al-doped HfO_2 samples, as was expected, demonstrated a higher total amount of traps of $\approx 3.3 \times 10^{19}\,\text{cm}^{-3}$. At 77 K the density of occupied traps significantly increases to $\approx(6.0\text{–}7.7) \times 10^{19}\,\text{cm}^{-3}$, following a similar annealing dependence trend. This behavior of HfO_2 trapping properties suggests that O vacancies play an insignificant role in charge trapping as their concentration is expected to increase in the samples annealed in O-free ambient rather than to decrease. It is more likely that defects responsible for trapping phenomena in HfO_2 have polaronic nature, which is addressed in more detail below.

2. Photodepopulation study

Results of photodepopulation experiments are described below and allow one to infer the energy distribution of deep traps in the studied HfO_2 films. Amorphous samples (undoped and Al-doped HfO_2) are compared in Fig. 4, and results for samples annealed at 850 °C (undoped and Al-doped HfO_2) and 1000 °C (undoped and Si-doped HfO_2) are shown in Figs. 5 and 6, respectively. In the undoped uncharged amorphous HfO_2 sample [Figs. 4(a) and 4(c), black curves] almost no charge variation was observed for photon energies less than 4 eV. However, in all other samples in the uncharged state [black curves in Figs. 4(b), 4(d), 5, and 6] net electron detrapping was detected between 2 and 3.5 eV. This shows that some deep electron traps were already filled during sample fabrication. Above 4.5 eV electron trapping was detected in all uncharged samples (black curves in Figs. 4–6) as internal photoemission (IPE) of electrons from the Si valence band into the SiO_2/HfO_2 stack becomes possible (IPE onset is indicated in Figs. 4–6 by blue dashed lines). This effect can be suppressed in charged samples (red curves in Figs. 4–6) due to repulsive field of electrons trapped in the HfO_2 film that prevents photoinjection of electrons from the Si substrate. Above ∼5.6 eV, generation of electron-hole pairs in the oxide begins to occur, leading to elimination of the rest of the trapped electrons and the appearance of the net positive charge in illuminated samples. The negative V_{fb} shift observed in charged doped samples after relaxation (Figs. 5 and 6, right panels, red curves) is another indicator of the presence of filled deep traps in as-fabricated samples, which are annihilated during charging pulse due to impact ionization. At the same time, injected electrons are captured by more shallow traps and, therefore, susceptible to thermal detrapping during relaxation.

Overall, in all samples most of the photoactive deep traps seem to be distributed between 2 and 3.5 eV below the HfO_2 conduction band, in agreement with the previously published results [11,15,16,23]. The spectral component close to 4 eV cannot be reliably quantified because of concomitant photoinjection from Si in the same spectral range. No significant influence of annealing or doping on trapping at room temperature is observed. This suggests that the traps are related to localized electron states of intrinsic origin.

3. Thermal emission study

The next part of the experimental section addresses the thermally activated emission experiments. The notable decrease of flat-band voltage after cooling the annealed samples to 77 K, as illustrated in Fig. 7(b), likely results from discharging of electron traps at the Si/SiO_2 interface (Si dangling bonds, often referred to as P_b-type centers) as the p-Si Fermi level shifts towards the Si valence band edge [24,25]. The schematic of this effect as well as the impact of interface traps recharging on the flat-band voltage shift in detrapping experiments (which is calculated with respect to the initial V_{fb} value at room temperature) are illustrated in Fig. 7 (on the example of undoped HfO_2 samples annealed at 850 °C for 60 s). For the unannealed samples this effect was not observed because interface traps were effectively passivated by hydrogen during atomic layer deposition of the HfO_2 film.

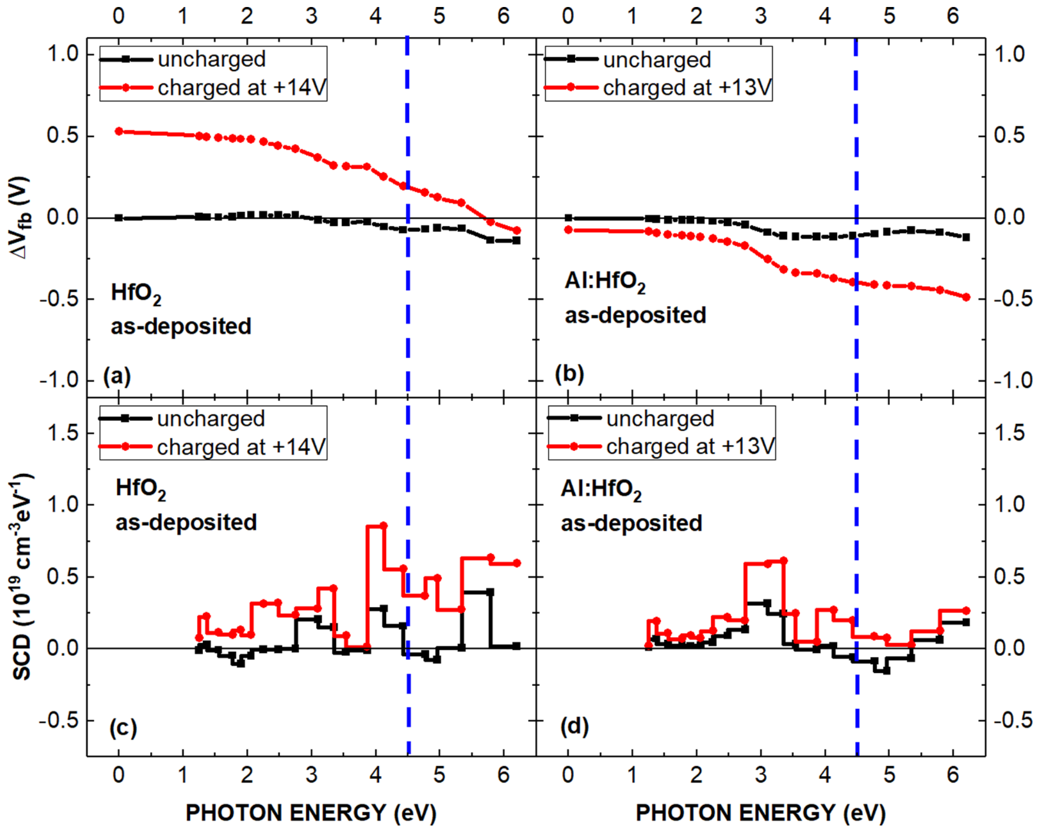

FIG. 4. V_{fb} shift variation due to optical excitation [panels (a) and (b)] and spectral charge density diagrams [panels (c) and (d)] as measured on as-deposited HfO_2 and Al:HfO_2 samples in the uncharged state (black curves) and after charging pulse of indicated amplitude and ⩾48 h relaxation (red curves). Flat-band voltage shift is measured with respect to the initial V_{fb} value measured at room temperature before charging. Vertical dashed lines mark the energy onset of electron emission from Si valence band over a 7.5-nm-thick SiO_2 [17]. Negative SCD values correspond to net electron trapping in the SiO_2/HfO_2 stack.

By contrast, during high temperature annealing in N_2 most Si-H bonds are expected to be broken and interface traps become electrically active again [26]. Therefore, the flat-band voltage shift variation measured for the annealed samples was recalculated in order to account for the interface traps recharging effect [Fig. 7(c)]. The V_{fb} shift variation due to the interface trap re-charging (open circles) was subtracted from the V_{fb} shift variation measured on the charged samples in thermally activated emission experiments (filled squares), resulting in the V_{fb} shift variation induced solely by thermal detrapping of electrons from electron traps in HfO_2 (open squares).

One of the main parameters measured during thermally activated emission experiments is a thermal detrapping rate dV_{fb}/dt, which is defined as a change in the flat-band voltage between two consequent measurements of V_{fb} and T divided by the time between these V_{fb} and T readouts. By plotting the detrapping rate as a function of sample temperature the characteristic energy depth of filled traps E_{tr} may be estimated from an electron detrapping rate peak position T_{peak} using the following expression [27]:

$$E_{tr} \sim kT_{peak}\ln(\nu\tau), \tag{3}$$

where ν is the typical optical phonon frequency in HfO_2 (about 10^{13} Hz as taken from Ref. [28]) and $\tau \approx 10^4$ s is the estimated detrapping time in the studied temperature range. The latter is the upper limit which is equal to the typical time scale of the thermally activated emission experiment. The precise value of τ and its T dependence is not known, nevertheless, one would not expect possible errors to exceed 5–10% since τ is entering Eq. (3) under logarithm. This approach is further illustrated in Fig. 8. We note that trapping energies E_{tr} calculated using Eqs. (2) and (3) have the meaning of the average (characteristic) thermal depth of traps in a sample. By contrast, the activation energy E_a, used in Fig. 8(c), defines the energy depth of a group of traps in a certain temperature interval. That explains why for calculation of E_{tr} the detrapping rate peak position T_{peak} is used.

Results of electron injection at 77 K and thermally activated emission experiments are summarized in Figs. 9–11 for as-deposited samples, those annealed at 850 °C for 60 s or annealed at 1000 °C for 30 s, respectively. The flat-band voltage variation rate dV_{fb}/dt versus temperature curves are shown in panels (a) and (b). They correspond to the charge density variation rate which allows one to estimate the characteristic thermal energy depth of traps by using Eq. (3). Panels (c) and (d) demonstrate V_{fb} variation with temperature for samples after electron injection at 77 K and, also, for the reference uncharged sample (open circles) to eliminate the effect of interface traps recharging [as explained earlier in relationship to Fig. 7(c)]. It was noticed that in the undoped samples V_{fb} variation rate peaks shift from ≈170 K and ≈195 K in

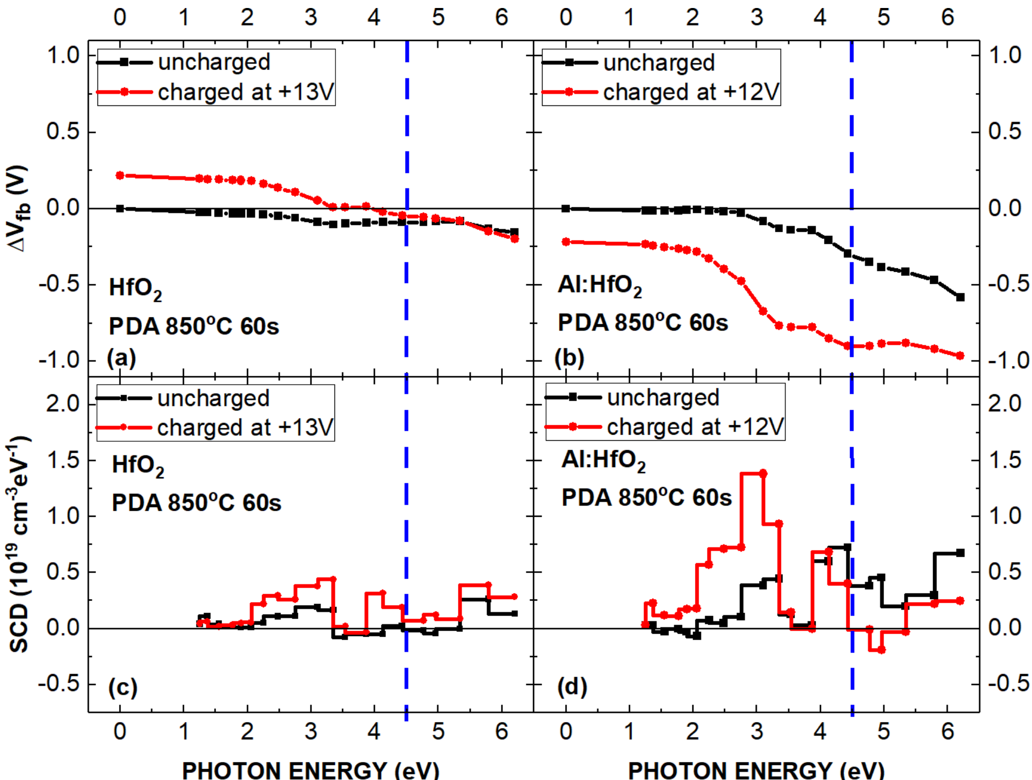

FIG. 5. V_{fb} shift variation due to optical excitation [panels (a) and (b)] and spectral charge density diagrams [panels (c) and (d)] as measured on HfO_2 and Al:HfO_2 samples annealed for 60 s at 850 °C in the uncharged state (black curves) and after charging pulse of indicated amplitude and $\geqslant$48 h relaxation (red curves). Flat-band voltage shift is measured with respect to the initial V_{fb} value measured at room temperature before charging. Vertical dashed lines mark the energy onset of electron emission from Si valence band over a 7.5-nm-thick SiO_2 [17]. Negative SCD values correspond to net electron trapping in the SiO_2/HfO_2 stack.

amorphous (unannealed) samples [Fig. 9(a)] to ≈180–190 K [Fig. 10(a)] and ≈208 K [Fig. 11(a)] in the crystallized ones. These results correspond to the increase of the average trap depth E_{tr} from ~0.57 eV and ~0.66 eV to ~0.61–0.64 eV and ~0.70 eV, respectively. Therefore, it may be concluded that this trap energy distribution is also affected by annealing. In doped samples [Figs. 10(b) and 11(b)] we observe similar detrapping rate peak positions at ≈180–190 K and at ≈216 K, corresponding to average $E_{tr} \sim 0.61 - 0.64$ eV and ~0.73 eV. This result once again indicates that doping has no substantial impact on electron trapping in HfO_2 films pointing to the intrinsic nature of the trapping sites. No significant difference between two biasing conditions [$V_{hold} = -5$ V (red squares and blue circles) and $V_{hold} = V_{fb}$ (black + and × symbols)] was observed indicating that the impact of annihilation by unfrozen holes is negligible. Another important feature revealed by these experiments is significant detrapping occurring already at 77 K during 4–5 h relaxation after the charging pulse. This suggests the presence of high density of even more shallow traps, which can be thermally ionized at this low temperature ($E_{tr} < 0.2$ eV).

4. Overview of experimental results

These results demonstrate a broad spectrum of electron trapping sites present in undoped HfO_2 layers. These include not only deep states with *optical* depopulation energies in the 2.0–3.5-eV range, but also traps which are *thermally* depopulated with activation energies below 0.7 eV. Furthermore, there are indications of shallow traps with thermal ionization energies in the range of 0.2 eV which are thermally depopulated at 77 K. The relation between optical and thermal ionization energies for these traps has been discussed in Refs. [12,16]. In a nutshell, the photodepopulation energies of electron traps into CB states above the mobility edge are expected to be 2.2 times larger than the thermal ionization energies into the CB edge states. Thus, traps with thermal ionization energies of 0.7 eV can be optically ionized by photon energies of about 1.6 eV. Our results also indicate that trap densities appear to be insensitive to the presence of dopants (Al, Si), suggesting their intrinsic nature. The observed reduction of the trap density with the temperature of annealing in O-free ambient allows one to exclude O deficiency of HfO_2 as the primary source of electron trapping.

To understand these data, we note that the samples studied here typically contain crystalline regions of non-FE (monoclinic, tetragonal, cubic) and orthorhombic FE phases intermixed with amorphous regions, similar to a model proposed for amorphous oxide semiconductors (see Ref. [29], Fig. 8). Some of the trap energies are consistent with those predicted for electron polarons in m-HfO_2 ($E_{tr} \sim 0.2$ eV) [30] and polaron and bipolaron photodepopulation energies in the bulk of amorphous HfO_2 (2.0–3.5 eV) [12,16]. In addition, our samples most likely contain boundaries between non-FE and FE grains and amorphous regions. Simple symmetric grain boundaries (GBs), such as Σ3 and Σ5, have been shown

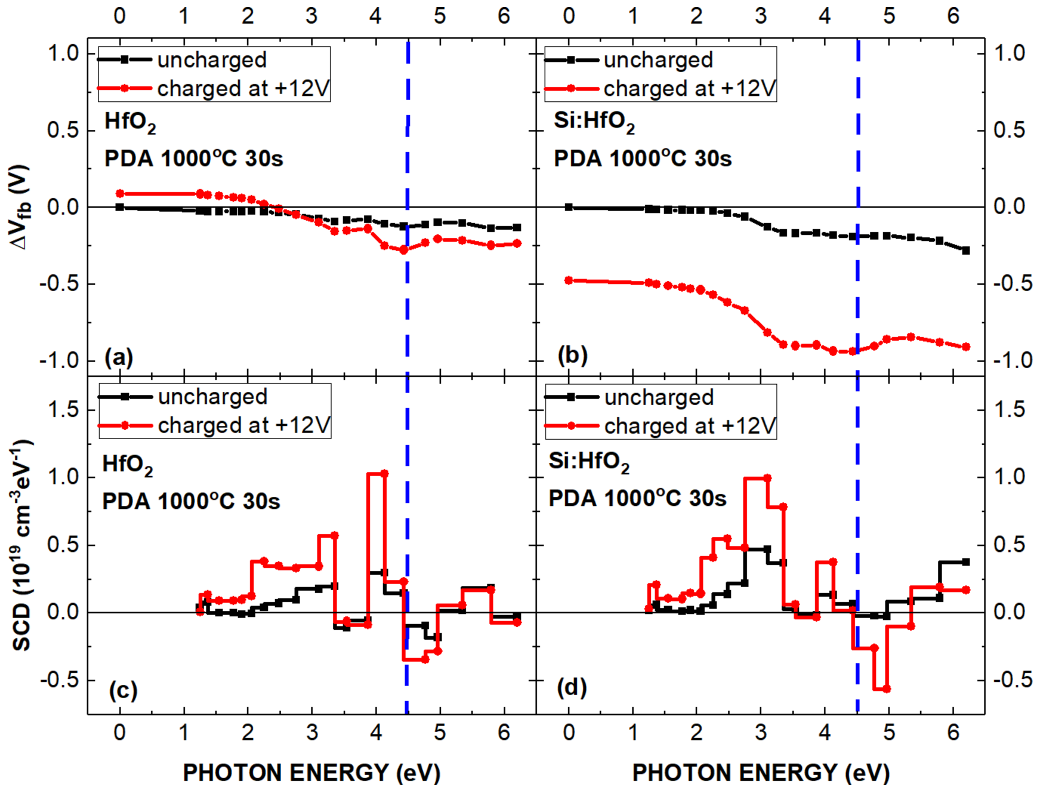

FIG. 6. V_{fb} shift variation due to optical excitation [panels (a) and (b)] and spectral charge density diagrams [panels (c) and (d)] as measured on HfO_2 and Si:HfO_2 samples annealed for 30 s at 1000 °C in the uncharged state (black curves) and after charging pulse of indicated amplitude and ⩾48 h relaxation (red curves). Flat-band voltage shift is measured with respect to the initial V_{fb} value measured at room temperature before charging. Vertical dashed lines mark the energy onset of electron emission from Si valence band over a 7.5-nm-thick SiO_2 [17]. Negative SCD values correspond to net electron trapping in the SiO_2/HfO_2 stack.

theoretically to induce interface states in a range of about 0.3 eV near the conduction band minima of monoclinic or cubic phases [31–33]. Upon trapping an electron, these states can become deeper traps due to lattice polarization of the high-k HfO_2 matrix. This has been demonstrated for the case of hole trapping at in-plane and stepped ZrO_2 and HfO_2 surfaces [34]. Recent experimental results demonstrate that GBs have more complex atomic structures of the interface with a few

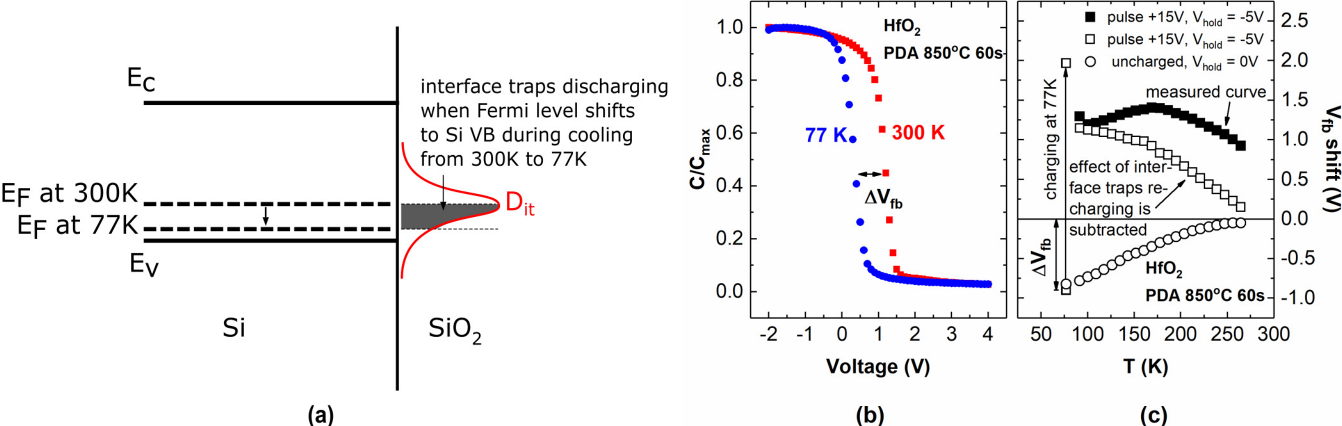

FIG. 7. (a) Schematics of interface traps discharging in annealed samples during cooling down from room temperature to 77 K (the hatched area represents the density of interface traps that emit electrons into the substrate due to the Fermi level shift); (b) 100 kHz CV curves measured on the annealed HfO_2 sample at 300 and 77 K before charging, illustrating V_{fb} shift corresponding to interface traps discharge; (c) V_{fb} shift (with respect to the initial V_{fb} value at room temperature) variation with temperature in annealed HfO_2 samples after charge injection at 77 K due to thermal detrapping with (■) and without (□) effect of interface traps recharging, and V_{fb} shift variation in the uncharged sample representing the effect of interface traps recharging (○).

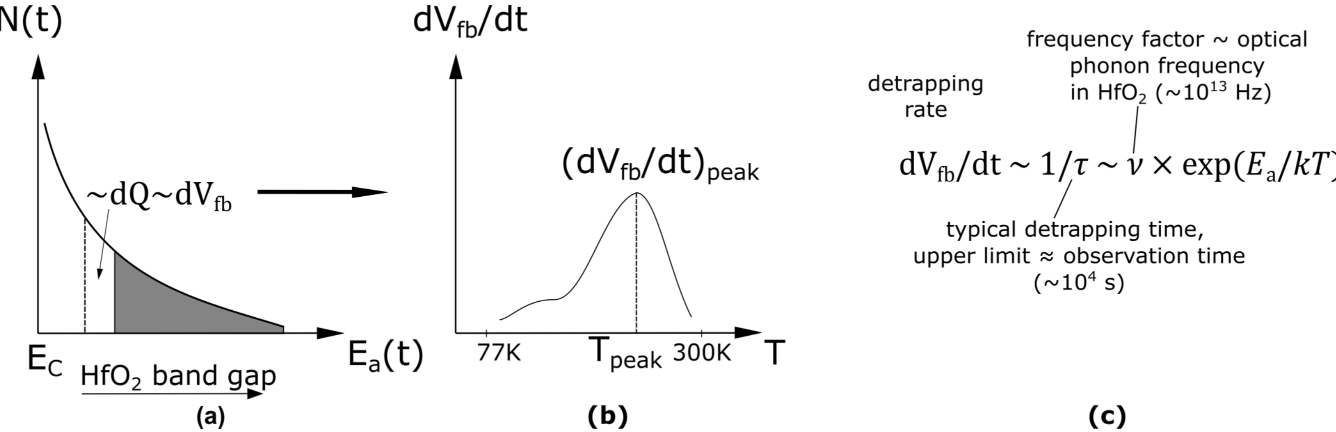

FIG. 8. (a) Schematic distribution of the density of gap states $N(t)$ in (amorphous) hafnia; (b) an expected detrapping rate variation; and (c) the relation between the thermal detrapping rate and the characteristic range of thermal activation energies of traps.

undercoordinated oxygen or hafnium ions at the grain boundary [35].

Thus, the coordination of Hf and O ions at surfaces, grain boundaries, and in the amorphous phase as well as the lattice polarization has been shown to play the major role in electron and hole trapping in these materials. Therefore, as a preliminary model, we propose that at 77 K electrons are initially trapped in shallow polaron states in monoclinic and

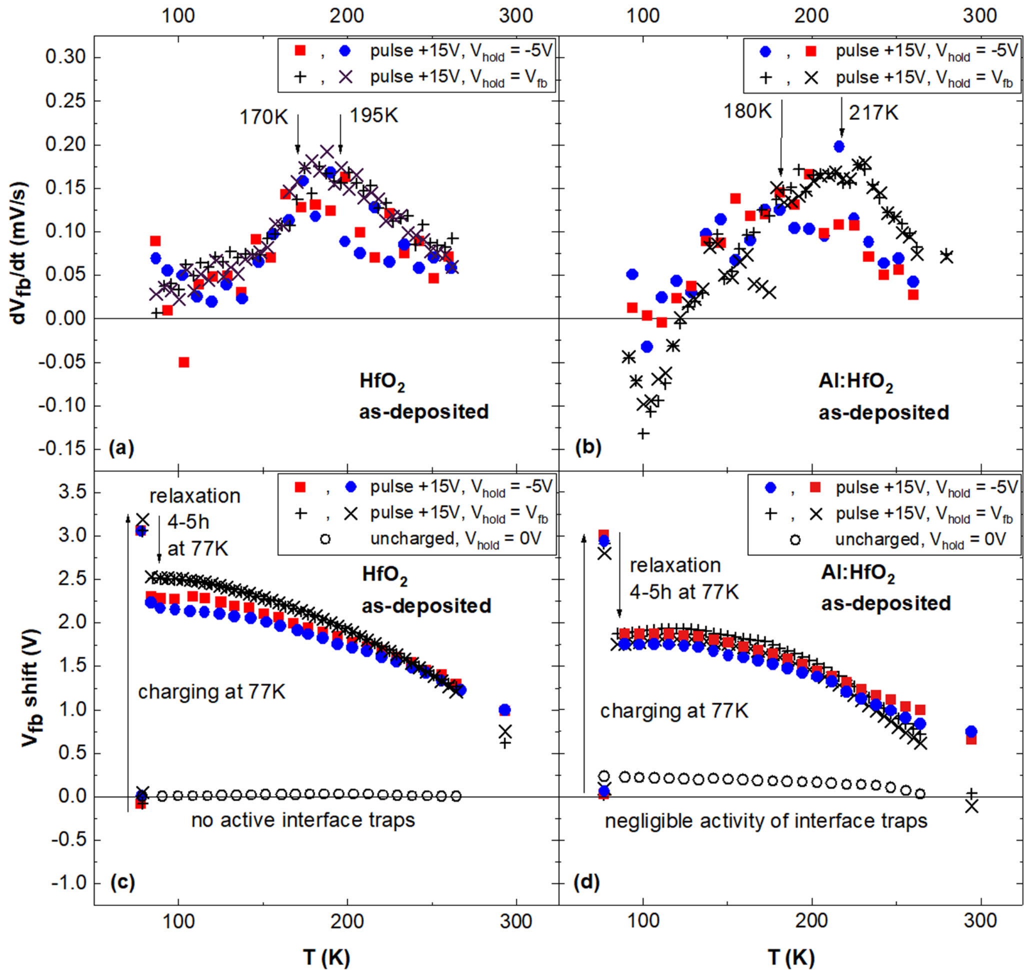

FIG. 9. Flat-band voltage variation rate [panels (a) and (b)] and flat-band voltage shift with respect to the initial V_{fb} value at room temperature [panels (c) and (d)] versus temperature as measured on as-deposited (undoped and Al-doped) HfO_2 samples. Measurements were repeated twice under "holding" voltages of −5 V and at the flat-band condition during sample heating. Additional measurements for uncharged samples were conducted under zero bias during sample heating.

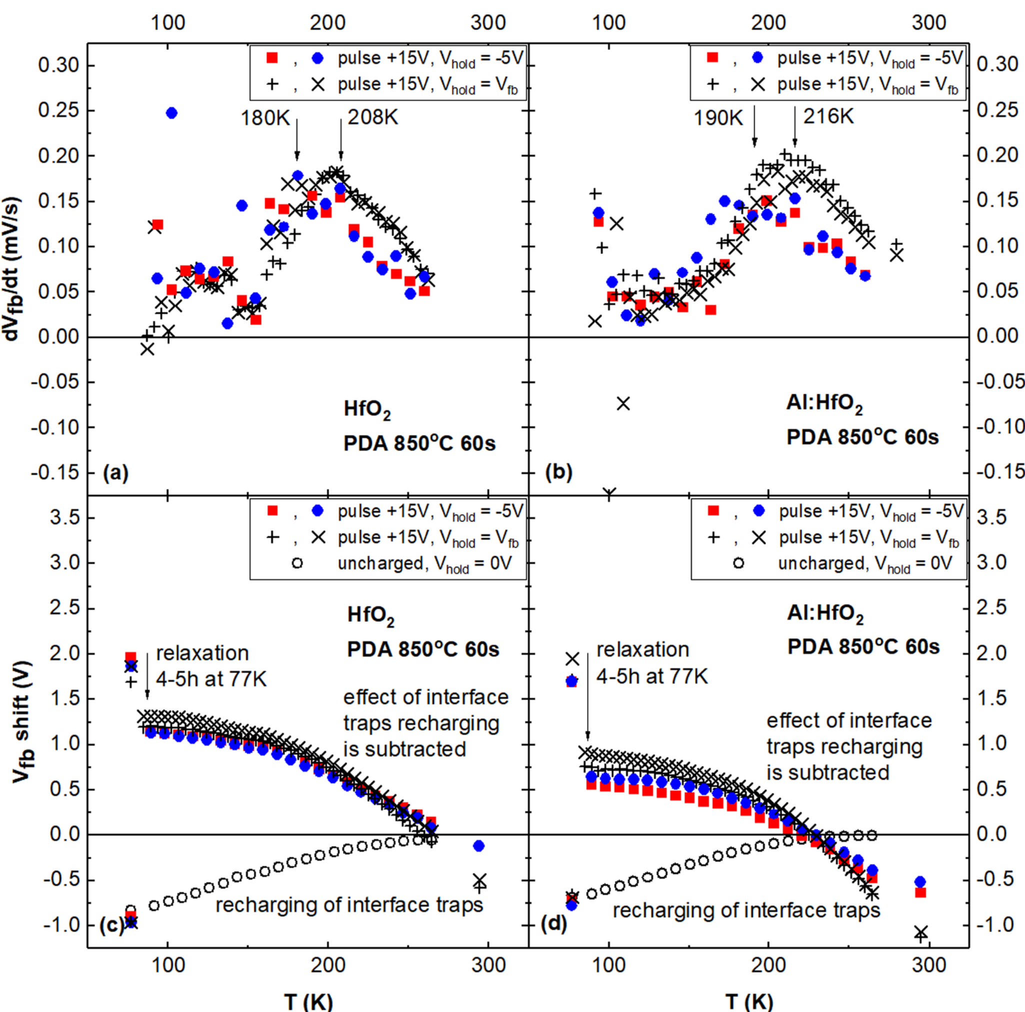

FIG. 10. Flat-band voltage variation rate [panels (a) and (b)] and flat-band voltage shift with respect to the initial V_{fb} value at room temperature [panels (c) and (d)] versus temperature as measured on annealed at 850 °C for 60-s (undoped and Al-doped) HfO_2 samples. Measurements were repeated twice under holding voltages of −5 V and at the flat-band condition during sample heating. Additional measurements for uncharged samples were conducted under zero bias during sample heating.

orthorhombic HfO_2. Some of these electrons escape to an electrode while others do hop to grain boundaries and eventually end up in amorphous regions, where they are getting trapped at deeper states. To support this model, we discuss below the results of calculations for electron trapping at HfO_2 surfaces containing a range of undercoordinated atoms and distorted bonds which is relevant to the case of multicrystalline layers we analyze experimentally. We consider electron trapping properties of these surfaces to be analogous to GBs and more complex interfaces. A detailed study of these effects at interfaces between crystalline and amorphous phases will be reported in a separate publication.

B. Results of calculations

The three crystal phases and the corresponding surfaces considered in this work are shown in Table I. Surface termination introduces undercoordinated ions. For example, at the *m*-HfO_2 (−1 1 1) surface some Hf ions are six-coordinated by oxygen ions [see Fig. 12(a)], whereas the bulk coordination is 7. Even when the surface termination does not affect ion coordination of Hf, it still extends surface Hf-O bonds. To account for experimental conditions, an extra electron has been added to all surfaces and the resulting electron trapping energies are shown in Table I.

One can see that the electron trapping energies fall in the range 0.7–1.0 eV. We note that the trapping energies reported in Table I are calculated without defect image charge corrections. Image charge corrections for charged defects at surfaces are nontrivial, and standard methods that are used for bulk defects can fail [36]. Based on the high dielectric constant of HfO_2 and the cell dimensions used, we expect these corrections to be on the order of 0.1 eV.

We note that, as predicted in previous studies, the electron trapping occurs at the undercoordinated Hf ions present on the surface layer. These trapping energies are deeper than those calculated for bulk crystal, which are ∼0.2–0.3 eV for all three crystal phases studied in this work. The traps are not as deep as those predicted by our previous calculations for amorphous HfO_2 [16], which have an average trapping energy of 1.0 eV. The spin density of a trap is plotted in Fig. 12(b). The electron is localized over 2 Hf ions, as is quite typical for polaronlike electron states in HfO_2 [16], although

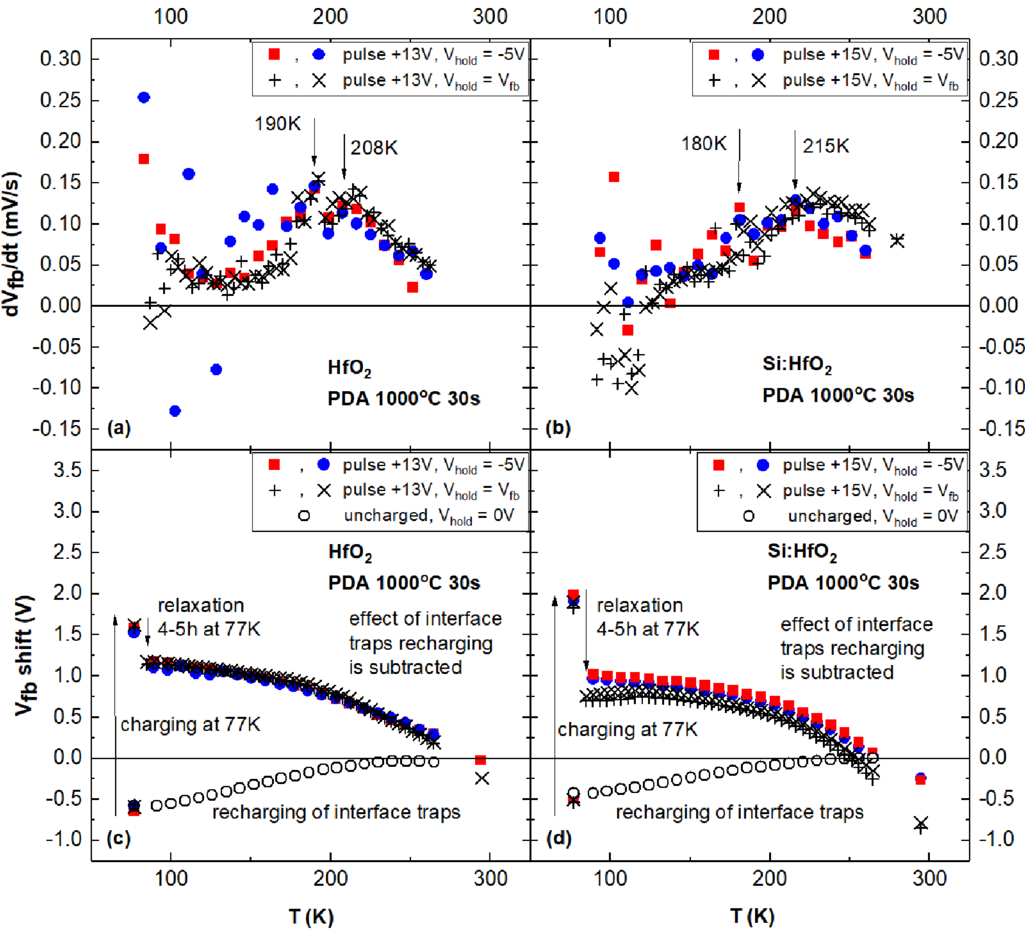

FIG. 11. Flat-band voltage variation rate [panels (a) and (b)] and flat-band voltage shift with respect to the initial V_{fb} value at room temperature [panels (c) and (d)] vs temperature as measured on annealed at 1000 °C for 30-s (undoped and Si-doped) HfO_2 samples. Measurements were repeated twice under holding voltages of −5 V and at the flat-band condition during sample heating. Additional measurements for uncharged samples were conducted under zero bias during sample heating.

in some cases the distribution is not symmetric and one Hf ion is preferred. On average, the Kohn-Sham one-electron-state of surface trap is ∼1.6 eV below the CBM, with a spread of approximately 0.2 eV. Most of the trapping sites are also capable of trapping a second electron. The electron-electron repulsion is compensated by the increased lattice polarization [12,16]. The trapping energies of the second electron fall within the same range as the first trapping energies. Therefore, the trapping energy of an electron is quite independent (to within 0.3 eV) of the crystal phase and whether or not the electron is trapped into a single- or a bielectron trap.

TABLE I. Electron trapping energies at surfaces in monoclinic, tetragonal, and orthorhombic phases of HfO_2.

Crystal structure	Surface	E_{tr} (eV)
Monoclinic	(1 1 1)	0.8
	(−1 1 1)	1.0
Tetragonal	(1 0 0)	0.8
	(0 0 1)	0.8
Orthorhombic	(1 0 0)	0.8
	(0 0 1)	0.7

We have also analyzed how electron trapping energy can depend on the position of the trap site with respect to the surface. For the m-HfO_2 (−1 1 1) surface and t-HfO_2 (1 0 0) surface we simulated a trap that is in a sublayer just one layer of atoms deep into the slab. For the t-HfO_2 (1 0 0) surface, we find that the electron trapping energy is 0.05 eV lower. For the m-HfO_2 (−1 1 1) surface, however, trapping energies at the subsurface are 0.5 eV lower than at the surface (resulting in a trapping energy of 0.5 eV). These results are consistent with the bulk values.

Thus, our calculations show that surface trap stability falls broadly within the same range regardless of the specific crystal structure and that undercoordination and bond distortion are the critical parameters determining the depth of trapped states.

IV. CONCLUSION

Experimental study of electron trapping in ferroelectric (Si- and Al-doped) HfO_2 indicates no significant contribution of the dopants to the density of electron traps as compared to the undoped reference insulating films.

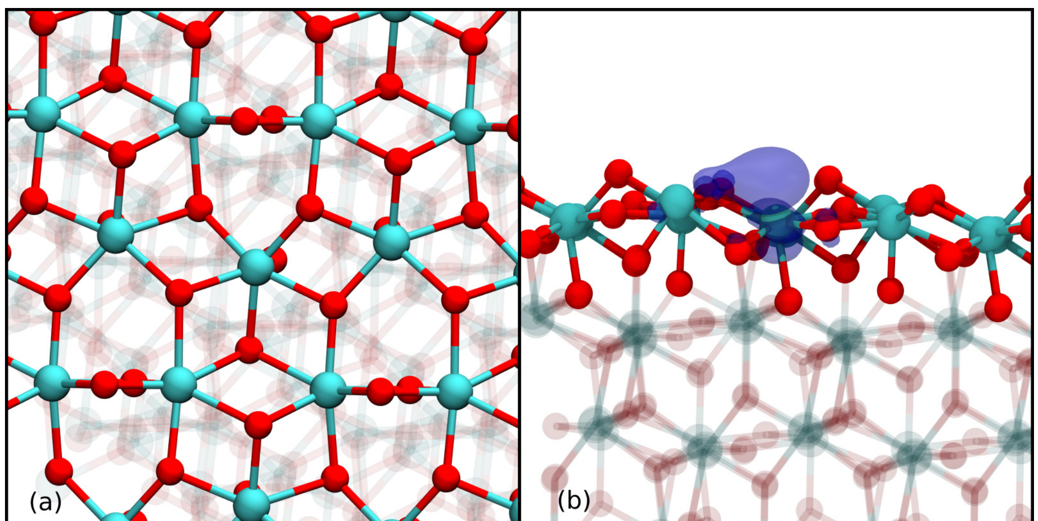

FIG. 12. (a) Shows the top layer of the (−1 1 1) surface of *m*-HfO_2. Hf ions are colored light blue and O ions are colored red. (b) A close (side on) view of the single electron trap in the monoclinic (−1 1 1) surface. The dark blue surface corresponds to an isosurface (= 0.005) of the spin density.

These traps are predominantly of intrinsic nature and are distributed in a wide energy range across the HfO_2 band gap. The room temperature experiments reveal the presence of deep traps. Their volume concentration slightly decreases from (2–3) $\times 10^{19}$ cm^{-3} in as-deposited mostly amorphous hafnia to (1.5–2) $\times 10^{19}$ cm^{-3} in films crystallized by high-temperature annealing in oxygen-free ambient. This behavior suggests the trapping sites are related to morphology and disorder in HfO_2 films rather than to the oxygen deficiency. The energy distribution of some of the traps (optical depth 2–3.5 eV below the CB bottom of HfO_2) is consistent with them being deep polaronic states in *a*-HfO_2 regions. In addition, we found that HfO_2 interface states may have electron trapping energies of ∼0.6–1.0 eV, consistent with the experimental thermal ionization energies. Photodepopulation energies of these states should be in the range of ∼1.5–2.2 eV [12,16]. On the other hand, the concentration of these traps appears to be much higher, in the range (6–7) $\times 10^{19}$ cm^{-3}, without significant sensitivity to the crystallization anneal or the film doping by Si or Al. Based on the similarity of thermal trap depth energies, close to 0.6–0.7 eV, we propose these defects to be also of polaronic origin but associated with more ordered grain boundaries of HfO_2 nanocrystallites. Small sensitivity of the trapping energy to the particular crystal phase of HfO_2 predicted by DFT calculations supports this hypothesis. These results, in combination with previous findings of the (bi)polaronic nature of deep traps in *a*-HfO_2 layers, allow us to propose an atomistic model to describe the trapping phenomena in hafnia films.

The broad range of discovered defect energies, as revealed by DFT calculations, explains quite well the observed electron trapping in both thermal ionization (0.7–1.0 eV below HfO_2 CB) and photoionization energy range (2.0–3.5 eV below the HfO_2 CB). Therefore, the results of DFT calculations support a polaron model of electron trapping in HfO_2 layers based on the intrinsic nature of both shallow and deep electron traps, which was further confirmed by negligible sensitivity of experimental results to the doping of the studied layers.

[1] T. S. Böscke, J. Müller, D. Bräuhaus, U. Schröder, and U. Böttiger, Appl. Phys. Lett. **99**, 102903 (2011).

[2] J. Müller, E. Yurchuk, T. Schlösser, J. Paul, R. Hoffmann, S. Müller, D. Martin, S. Slezaceck, P. Polyakovski, J. Sundquist, M. Czernohorsky, K. Seidel, P. Kucher, R. Boshke, M. Trentzsch, K. Gebauer, U. Schröder, and T. Mikolajick, in *2012 Symposium on VLSI Technology (VLSIT)* (IEEE, Honolulu, HI, 2012), pp. 25–26.

[3] J. Müller, P. Polakowski, S. Mueller, and T. Mikolajick, ECS J. Solid State Sci. Technol. **4**, N30 (2015).

[4] V. V. Afanas'ev and A. Stesmans, J. Appl. Phys. **95**, 2518 (2004).

[5] G. Bersuker, J. H. Sim, C. S. Park, C. D. Young, S. V. Nadkarni, R. Choi, and B. H. Lee, IEEE Trans. Device Mater. Rel. **7**, 138 (2007).

[6] A. Kerber and E. A. Cartier, IEEE Trans. Device Mater. Rel. **9**, 147 (2009).

[7] T. Ando, Materials **5**, 478 (2012).

[8] E. Yurchuk, J. Müller, S. Müller, J. Paul, M. Pešić, R. van Bentum, U. Schröder, and T. Mikolajick, IEEE Trans. Electron Devices **63**, 3501 (2016).

[9] A. S. Konashuk, E. O. Filatova, S. S. Sakhonenkov, N. M. Kolomiiets, and V. V. Afanas'ev, J. Phys. Chem. C **124**, 16171 (2020).

[10] A. Stesmans and V. V. Afanas'ev, Microelectron. Eng. **178**, 112 (2017).

[11] F. Cerbu, O. Madia, D. V. Andreev, S. Fadida, M. Eizenberg, L. Breul, J. G. Lisoni, J. A. Kittl, J. Strand, A. L. Shluger, V. V. Afanas'ev, M. Houssa, and A. Stesmans, Appl. Phys. Lett. **108**, 222901 (2016).

[12] J. Strand, M. Kaviani, D. Gao, A. El-Sayed, V. V. Afanas'ev, and A. L. Shluger, J. Phys.: Condens. Matter **30**, 233001 (2018).
[13] V. V. Afanas'ev and A. Stesmans, Phys. Rev. B **59**, 2025 (1999).
[14] W. C. Wang, M. Badylevich, V. V. Afanas'ev, A. Stesmans, C. Adelmann, S. Van Elshocht, J. A. Kittl, M. Lukosius, Ch. Walczyk, and Ch. Wenger, Appl. Phys. Lett. **95**, 132903 (2009).
[15] V. V. Afanas'ev, W. C. Wang, F. Cerbu, O. Madia, M. Houssa, and A. Stesmans, ECS Trans. **64**, 17 (2014).
[16] J. Strand, M. Kaviani, V. V. Afanas'ev, J. G. Lisoni, and A. L. Shluger, Nanotechnology **29**, 125703 (2018).
[17] V. V. Afanas'ev and A. Stesmans, Appl. Phys. Lett. **81**, 1053 (2002).
[18] T. D. Kühne, M. Iannuzzi, M. Del Ben, V. V. Rybkin, P. Seewald, F. Stein, T. Laino, R. Z. Khaliullin, O. Schütt, F. Schiffmann, D. Golze, J. Wilhelm, S. Chulkov, M. H. Bani-Hashemian, V. Weber, U. Borštnik, M. Taillefumier, A. S. Jakobovits, A. Lazzaro, H. Pabst *et al.*, J. Chem. Phys. **152**, 194103 (2020).
[19] M. Guidon, J. Hutter, and J. Van de Vondele, J. Chem. Theory Comput. **5**, 3010 (2009).
[20] J. VandeVondele and J. Hutter, J. Chem. Phys. **127**, 114105 (2007).
[21] M. Krack, Theor. Chem. Acc. **114**, 145 (2005).
[22] M. Guidon, J. Hutter, and J. Van de Vondele, J. Chem. Theory Comput. **6**, 2348 (2010).
[23] L. Vandelli, A. Padovani, L. Larcher, R. G. Southwick, W. B. Knowlton, and G. Bersuker, IEEE Trans. Electron Devices **58**, 2878 (2011).
[24] P. V. Gray and D. M. Brown, Appl. Phys. Lett. **8**, 31 (1966).
[25] A. Beckers, F. Jazaeri, and C. Enz, IEEE Trans. Electron Devices **65**, 3617 (2018).
[26] A. Stesmans, J. Appl. Phys. **88**, 489 (2000).
[27] S.-D. Tzeng and S. Gwo, J. Appl. Phys. **100**, 023711 (2006).
[28] E. Anastassakis, B. Papanicolaou, and I. M. Asher, J. Phys. Chem. Solids **36**, 667 (1975).
[29] J. E. Medvedeva, D. B. Buchholz, and R. P. H. Chang, Adv. Electron. Mater. **3**, 1700082 (2017).
[30] D. M. Ramo, A. L. Shluger, J. L. Gavartin, and G. Bersuker, Phys. Rev. Lett. **99**, 155504 (2007).
[31] K. P. McKenna and A. L. Shluger, Proc. R. Soc. A **467**, 2043 (2011).
[32] E. Degoli, E. Luppi, and N. Capron, J. Nanomater. **2017**, 2404378 (2017).
[33] K.-H. Xue, P. Blaise, L. R. C. Fonseca, G. Molas, E. Vianello, B. Traore, B. De Salvo, G. Ghibaudo, and Y. Nishi, Appl. Phys. Lett. **102**, 201908 (2013).
[34] M. J. Wolf, K. P. McKenna, and A. L. Shluger, J. Phys. Chem. C **116**, 25888 (2012).
[35] S. Petzold, A. Zintler, R. Eilhardt, E. Piros, N. Kaiser, S. U. Sharath, T. Vogel, M. Major, K. P. McKenna, L. Molina-Luna, and L. Alff, Adv. Electron. Mater. **5**, 1900484 (2019).
[36] H. P. Komsa and A. Pasquarello, Phys. Rev. Lett. **110**, 095505 (2013).